Mixture design of an environmentally friendly scale and corrosion inhibitor in reclaimed wastewater for cooling systems

Juntao Jin[a,b], Mingyuan Li[b], Yuntao Guan[a,*]

[a]*Graduate School at Shenzhen, Tsinghua University, Shenzhen 518055, Guangdong, China, Tel./Fax: +86 755 23965080; email: 422362086@qq.com (J. Jin), Tel. +86 755 26036702; Fax: +86 755 26036511; email: guanyt@tsinghua.edu.cn (Y. Guan)*
[b]*Shenzhen Urban Planning & Resource Research Center, Shenzhen, Guangdong 518055, China, Tel./Fax: +86 755 23965080; email: 342248231@qq.com (M. Li)*

ABSTRACT

An environmentally friendly inhibitor was designed by the mixture design method and its application in a pilot-scale cooling system with reclaimed wastewater as the makeup water was evaluated. The optimized composition of the inhibitor was 12.5% PBTCA, 21.8% $ZnSO_4$, 18.7% PASP, 9.4% HPAA, 18.8% AA-ATMP-HPA polymer, and 18.8% HPMA. The inhibition efficiencies of carbonate scale and corrosion were 93.3 and 94.4%, respectively. The scale inhibition was due to the distorted crystal formation of the scale through the action of carboxyl and phosphonic acid groups in the inhibitor. The corrosion inhibition was attributed to the protective film formed by the adsorption of the inhibitor onto the surface of the carbon steel.

Keywords: Carbon steel; Inhibitor; Mixture design method; Cooling system; Reclaimed wastewater

1. Introduction

Reclamation of wastewater as the cooling water has received considerable attention due to the shortage of water resources [1–3]. However, reclaimed wastewater with high concentrations of organic matter and inorganic ions induce scale and corrosion readily in cooling systems [4]. In addition, the water components can be concentrated due to evaporation, exacerbating scale, and corrosion as a result of worsened water quality and increased water temperature [5]. Scale results in loss of capacity for thermal exchange, whereas corrosion involves deterioration of metallic surface, causing significant economic impacts. Hence, further researches on effective inhibitor for controlling scale and corrosion in cooling systems using reclaimed wastewater are necessary.

Many inhibitors have been used in order to address these problems. The use of polymers as scale and corrosion inhibitors has gained wide acceptance in recent years [6–15]. Polymers exhibit superior corrosion inhibition properties in contrast to simple organic molecules. The long chain carbon linkage and multiple adsorption sites of the polymers can adsorb on the metal surface and form a protecting film isolating the metal from the aggressive anions present in solution [16–18]. At the same time, polymers could prevent hard water systems from depositing mineral scale because of its strong complexation of functional

*Corresponding author.

groups and superior dispersion characteristic of macromolecule [19,20].

Polymer inhibitors tend to be compounded to achieve high efficiency and be more environment friendly since individual inhibitors have several short-comings, including high dosage, poor efficiency, and the development of drug resistance. For example, when used alone, polyaspartic acid (PASP) and 2-phosphonobutane-1,2,4-tricarboxylic acid (PBTCA) rarely achieve the desired anti-corrosion effects, especially in hard water and at high temperatures [20,21]. A more effective approach for preventing corrosion is to use inhibitors made from a mixture of chemicals. A number of researchers have evaluated the effect of inhibitors either synthesized from a single chemical or consisting of a main chemical and a secondary component [7–9,14,19,22,23]. Previous studies showed that these methods achieved suitable inhibition of scale and corrosion; however, some of these newly synthesized inhibitors may cause environmental problems. Other researchers have focused on the combined performance of more environment-friendly chemicals. For example, Zn^{2+} forms a metal-phosphonate-inhibiting film on the metallic surface when used in combination with 2-hydroxyl phosphonoacetic acid (HPAA), which is considered to be nontoxic to the environment [24,25]. Hydrolyzed polymaleicanhydride (HPMA) was found to be a more efficient scale and corrosion inhibitor compared with amino trimethylene phosphonic acid (ATMP) at the same concentration, while inhibition efficiencies of both HPMA and ATMP increased considerably with increasing Ca^{2+} concentrations [26]. It is likely that various combinations of chemicals can achieve the actually developed inhibition effects in an environmental way.

Inhibitor performance is highly dependent on water quality and contact time [27]; however, previous researchers have focused primarily on the inhibition effect of chemicals in artificial or simulated solutions [7,8,15,28]. Inhibition performance may be adversely affected when inhibitors are applied to real cooling systems, which experience changes in pH, temperature, and other water quality parameters. 1-Hydroxyethylidene-1, 1-diphosphonic acid (HEDP), and PBTCA at a dosage of 10 mg/L did not effectively control corrosion of carbon steel exposed to the reclaimed wastewater as makeup water for cooling tower systems [29]. However, at a dosage of 40 mg/L, HEDP, PBTCA, and ATMP showed high corrosion inhibition efficiency for carbon steel exposed to pretreated cooking wastewater as the makeup water [30]. Greater attention should be given to the inhibiting efficiency of inhibitors in reclaimed wastewater in cooling systems.

In this study, a reclaimed wastewater was collected from the Qishuyan Wastewater Treatment Plant in Changzhou, China and used as the cooling water. The raw water of Qishuyan was sanitary wastewater. The wastewater was treated by A2/O process and the quality of the effluent was up to China standards of reclaimed wastewater for cooling systems (Table 1). The corrosion inhibitor consisting of PBTCA, ZnSO₄, PASP, and HPAA was designed and optimized using the mixture design method in JMP software. In addition, scale inhibition performance was examined under different concentrations of HPMA and AA-ATMP-HPA used in conjunction with the corrosion inhibitor. The optimized scale and corrosion inhibitor was applied to a pilot-scale cooling system with reclaimed wastewater as the makeup water and evaluated its inhibition efficiency. Furthermore, the mechanism of inhibition was analyzed using electrochemical measurements, scanning electron microscopy (SEM), and Fourier transform infrared spectrometer (FTIR) analysis.

2. Materials and methods

2.1. Design of the inhibitor

PBTCA, PASP, HPAA, and ZnSO₄ were selected for inhibition of corrosion, while HPMA and AA-ATMP-HPA polymer were used as scale inhibitors because of their favorable chelation, threshold inhibition, and lattice distortion properties. All these compounds were analytical grade (Sinopharm Chemical Reagent Shanghai Co., Ltd, China).

The typical dosage of corrosion inhibitors was 15–30 mg/L [31] and the concentrations of phosphorus and zinc were limited to 0.5 and 10 mg/L, respectively [32]. To further reduce dosages and environmental influences while achieving high efficiency, the total dosage of the selected corrosion inhibitors in this study was limited to 10 mg/L, while the concentrations of phosphorus and zinc were limited to less than 0.5 and 2 mg/L, respectively. The boundaries of these limits were set by the following Eqs. (1)–(4):

$$0 \leq (x_1, x_3, x_4) \times 10 \leq 10 \tag{1}$$

$$(x_1 + x_2 + x_3 + x_4) \times 10 \leq 10 \tag{2}$$

$$\left(\frac{31}{270} \times x_1 + \frac{31}{156} \times x_4\right) \times 10 \leq 0.5 \tag{3}$$

$$\frac{65}{161} \times x_2 \times 10 \leq 2 \tag{4}$$

Table 1
Water quality characteristics of reclaimed wastewater used (units are in mg/L except for pH and *Fecal Coliform*)

Chemical and physical characteristics	Average value	Standards of reclaimed wastewater for cooling systems
pH	7.0	6.8–9.5
Chemical oxygen demand (COD)	20.4	≤100
Ammonia (NH_4^+)	0.32	≤10
Nitrate (NO_3^-)	9.7	–
Total phosphorus (TP)	0.35	–
Chloride (Cl^-)	66.2	≤700
Sulfate (SO_4^{2-})	94.5	≤1,800
Hardness (mg/L $CaCO_3$)	180	≤1,100
Total iron	0.06	≤1.0
Fecal coliform (CFU/L)	628	≤2,000

where x_1, x_2, x_3, and x_4 are percentages of PBTCA, $ZnSO_4$, PASP, and HPAA, respectively; 10 is total concentration of corrosion inhibitors; and 31, 270, 156, 65, and 161 are the relative molecular weights of phosphorus, PBTCA, HPAA, Zinc, and $ZnSO_4$, respectively.

A mixture design analysis with boundaries established by Eqs. (1)–(4) was conducted using the JMP software (SAS Institute Inc., Cary, NC, USA). A model based on the standard least squares approach was chosen to analyze and fit the experimental data [31]. Low dosages of HPMA and AA-ATMP-HPA (0, 1, 2, and 3 mg/L) were chosen to evaluate scale inhibition in the presence of corrosion-specific inhibitors.

2.2. Performance of the corrosion inhibitor

A rotating coupon corrosion test instrument (Motian, RC-III, China) was used to evaluate corrosion inhibition. Weight loss measurements were conducted to determine the corrosion inhibition efficiency. Carbon steel coupons with size of 10 mm × 1 mm × 650 mm were used. The chemical composition (wt.%) of carbon steel is as follows: C (0.17–0.23), Si (0.17–0.37), Mn (0.35–0.65), P (≤0.035), S (≤0.035), Ni (≤0.30), Cr (≤0.25), Cu (≤0.25), with the remainder as Fe. The precision of weight loss experiments was 0.01 mg. The volume of reclaimed wastewater was 1 L. The initial weight of each sample was recorded before immersion in the reclaimed wastewater, and the temperature of the solution was maintained in a water bath at 50 ± 1℃. The rotational speed of the samples was set using a speed regulator motor (Motian, Jiangsu, China).

The corrosion rate (v) of carbon steel was determined after 72 h of immersion at rotational speeds of 70–90 rpm using Eq. (5):

$$v = \frac{87,600\,W}{A\,\rho\,t} \tag{5}$$

where v is the corrosion rate (mm/yr), 87600 is a constant, W is the weight loss (g), A is the coupon area (cm^2), ρ is the density of carbon steel (g/cm^3), and t is the immersion time (h).

The corrosion inhibition efficiency (η) was calculated by Eq. (6):

$$\eta(\%) = \frac{v_0 - v_1}{v_0} \times 100 \tag{6}$$

where v_0 is the corrosion rate in the control solution (mm/yr), and v_1 is the corrosion rate in the solution with the addition of inhibitor (mm/yr).

2.3. Performance of the scale inhibitor

The experimental procedures used in static scale inhibition test and limited carbonate hardness test were described previously [32]. All the experiments were carried out in triplicate.

2.3.1. Static scale inhibition test

The scale inhibitor was added to 1-L volumetric flasks containing 750 mL of reclaimed wastewater. The pH was adjusted using 10-mL borax buffer solution (0.01 mol/L, pH 9). The solution was heated at 80 ± 1℃ until the volume was less than 250 mL, and then transferred into a 250-mL volumetric flask. Deionized water was added to the volumetric flask to a volume of 250 mL, after which the flask was sealed and heated at 80 ± 1℃ for 10 h. The concentrations of HCO_3^-, PO_4^{3-} and Zn^{2+} in the solution and their influences on

the formation of calcium carbonate, calcium phosphate, and zinc salt scales, were determined before adding the inhibitor as well as after heating. The control experiments without addition of inhibitor were conducted simultaneously. The scale inhibition efficiency (δ) was calculated by Eq. (7):

$$\delta\% = \frac{C_2 - C_1}{K\,C_0 - C_1} \times 100 \tag{7}$$

where C_0 is the chemical concentration before inhibitor addition (mg/L), C_1 is the chemical concentration without inhibitor after heating (mg/L), C_2 is the chemical concentration with inhibitor (mg/L), and K is the cycle of concentration.

All scale inhibition experiments were conducted in triplicate. The Ca^{2+} concentrations (as calcium carbonate) were standardized using the EDTA complexometry method described previously [32].

2.3.2. Limited carbonate hardness test

A 2-L scale inhibitor solution was prepared at the design concentration with reclaimed wastewater; half of the solution was used as the stock solution and the other half as the testing solution. The testing solution was heated to $80 \pm 1°C$ with a water bath. 30 mL of sample was collected every hour, after which the same volume of stock solution was added to maintain the constant volume. Concentrations of Cl^- and total alkalinity (as $CaCO_3$) were measured according to standard methods [32] and were used to calculate K (the cycle of concentration), K_M (the cycle of concentration of total alkalinity), and ΔK (the difference between K and K_M) through Eqs. (8)–(10). When ΔK was above 0.2, the cycle of concentration of reclaimed wastewater corresponds to the maximum concentration, and K is equal to the value of limited carbonate hardness.

$$K = \frac{C_{\text{cycle}}}{C_0} \tag{8}$$

$$K_M = \frac{M_{\text{cycle}}}{M_0} \tag{9}$$

$$\Delta K = K - K_M \tag{10}$$

where C_{cycle} is the concentration of Cl^- during cycle (mg/L), C_0 is the concentration of Cl^- in the stock solution (mg/L), M_{cycle} is the total alkalinity during cycle (mg/L, $CaCO_3$), and M_0 is the total alkalinity in the stock solution (mg/L $CaCO_3$).

2.4. Application of the inhibitor

The characteristics of the reclaimed wastewater are shown in Table 1. The total hardness of the reclaimed wastewater varied from 179 to 220 mg/L, making it "moderately hard" according to Galanakis et al. [33]. The conductivity ranged from 526 to 542 µS/cm, belonging to "almost hard" or "hard" categories. Concentrations of Cl^- ranged from 63 to 85 mg/L and SO_4^{2-} ranged from 64 to 101 mg/L, belonging to "almost hard" category. These results indicated that the reclaimed wastewater was likely to cause scale. The Larson–Skold Index (LI) (LI = ([Cl^-] + 2 [SO_4^{2-}])/[HCO_3^-]) defined the corrosiveness of water toward low-carbon steel and steel samples, which was used as a predictive indicator of iron corrosion [34]. If LI was above 1.2, an increasingly higher rate of localized corrosion would be observed. In this study, LI was calculated as 1.35–3.37, indicating a high corrosion potential for the carbon steel.

The pilot-scale cooling system is shown in Fig. 1. The test pipe was carbon steel as described in Section 2.2. Probes were placed at the inlet of the system to monitor conductivity and pH continuously during the experiment. For the pilot-scale cooling system, the flow rate was 200 L/h, the inlet temperature was 28°C, and the cycle of concentration was 3. The experiment time was 20 d. During the initial 2 d, the compound inhibitor (200 mg/L) was added for preconditioning purposes and then adjusted to 10 mg/L to simulate actual operation. The concentrations of Ca^{2+}, total iron, total hardness, and total alkalinity were determinate every 12 h. Carbon steel coupons were placed at the inlet and outlet of the system to evaluate corrosion rate and fouling resistance. Water quality and fouling resistance were measured according to standard methods described previously [32,35].

2.5. Mechanism of the inhibitor

2.5.1. Electrochemical measurement and SEM for corrosion inhibition mechanism

All electrochemical studies were conducted in a conventional three-electrode system (counter, reference, and working electrodes). The counter electrode was a platinum sheet with a surface area of 2 cm^2 and a saturated calomel electrode (SCE) was used as the reference. The working electrode was carbon steel (working surface area of 0.4 cm^2)—the electrode was abraded using emery paper of 1,200 grade prior to each experiment. The remaining area of the working electrode was covered with epoxy resin, with electrical
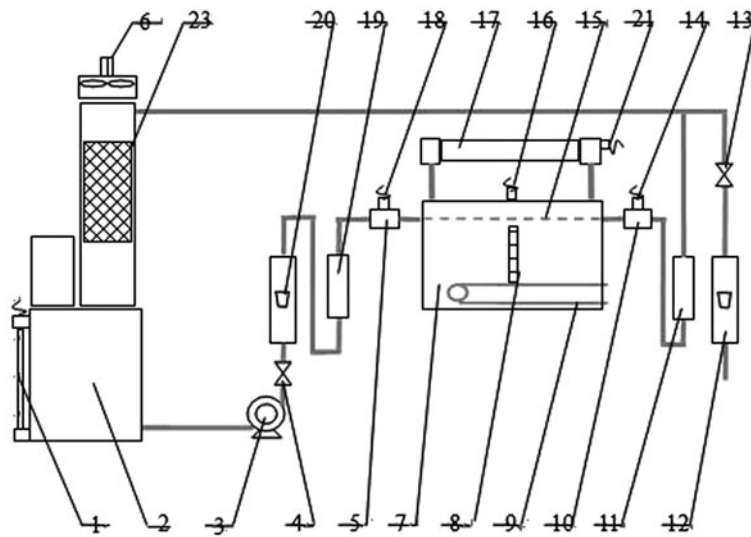
Fig. 1. Schematic diagram of the simulated cooling system.
Notes: (1) Water level meter; (2) water tank; (3) circulating pump; (4) control valve; (5) inlet chamber; (6) fan; (7) steam generator; (8) water level meter in boiler; (9) electric heater; (10) outlet chamber; (11) specimen holder in outlet; (12) discharge flow meter; (13) discharge control valve; (14) outlet thermometer; (15) test pipe; (16) steam thermometer; (17) condensing plant; (18) inlet thermometer; (19) specimen holder in inlet; (20) flow meter; (21) temperature sensor.

conductivity provided by a copper wire. All three electrodes were placed inside a glass cell, which was filled with reclaimed wastewater with or without inhibitor. The reclaimed wastewater was open to the atmosphere and the temperature was controlled at 50 ± 1℃ with water bath. During electrochemical measurements, the working electrode was immersed in the test solution for 30 min until a steady open-circuit potential was obtained. The electrochemical data were collected using a CHI 660D electrochemical analyzer under computer control. All potentials given in this study were calibrated with the reference electrode.

Electrochemical impedance spectroscopy (EIS) experiments were conducted over a frequency range of 10–100 kHz at an open-circuit potential of 5 mV. The EIS parameters were calculated by fitting the experimental results to an equivalent circuit using Zview software. Potentiodynamic polarization measurements were obtained at a scan rate of 1 mV/s and initiated at a potential of −1,000 mV to −2,000 mV vs. OCP after the working electrode reached a stable state (the OCP fluctuation was less than ±5 mV). Corrosion kinetic parameters were obtained automatically from the Tafel plots by Tafel extrapolation method using the CHI660D workstation analysis software. Measurements were performed three times to estimate the reproducibility under each experimental condition.

SEM (Hitachi, S-4800, Japan) was used to visualize the inhibitor film formed on the coupon surface and observe corrosion products after the weight loss test. The coupons and corrosion products were dried in a vacuum freeze drier overnight and coated with platinum before measurement.

2.5.2. SEM and FTIR for scale inhibition mechanism

In order to determine the morphology of different kinds of scales, calcium carbonate, calcium phosphate, and zinc salt were collected in a static scale inhibition test using artificial solutions with or without inhibitor. Calcium carbonate scale was prepared using the same procedure as the static scale inhibition test described in Section 2.3 with an artificial solution containing $CaCl_2$ and $NaHCO_3$ in deionized water (concentrations of Ca^{2+} and HCO_3^- were 250 mg/L). Calcium phosphate solutions were prepared using $CaCl_2$ and KH_2PO_4 (250 mg/L Ca^{2+} and 5 mg/L PO_4^{3-}). Zinc salt sale experiments were conducted with solutions containing $ZnSO_4·7H_2O$, $CaCl_2$, and $NaHCO_3$ (2.5 mg/L Zn^{2+}, 250 mg/L Ca^{2+}, and 250 mg/L HCO_3^-). The scales were dried in a vacuum freezer overnight and then coated with platinum before SEM measurements. Finally, a mixture of crystal deposits and KBr powder was compressed into a pellet and analyzed by the FTIR spectroscopy (Shimadzu, IRPrestige-21, Japan).

3. Results and discussion

3.1. Performance of the newly designed inhibitor

3.1.1. Corrosion inhibition performance

With the mixture design method in SAS JMP 9.0, optimal design and biquadratic interaction were determined using the boundaries described in Eqs. (1)–(4). Based on the fraction of the four compounds obtained from JMP, the inhibiting efficiency η was calculated (see Table 2). The highest inhibition efficiency was 90.5% for the four compounds mixture (solution number 20), while the lowest efficiency was 32.1% with only PASP or ZnSO$_4$ and PASP. The inhibition efficiency ranged from 32.1 to 72.2% for two compounds mixture, 53.4–83.4% for three compounds mixture, and 87.5–90.5% for four compounds mixture. These results suggest that a synergistic effect among the compounds exists, which can be attributed to adsorption competition or enhancement, as previously proposed by Aramaki and Hackerman [36]. In adsorption competition, the anion and cation are adsorbed at different sites on the metal surface; while in the adsorption cooperation, the anion is chemisorbed on the surface and the cation is adsorbed on the anion layer.

As shown in Fig. 2, a standard least squares approach in JMP was used to fit the inhibition efficiency. The predicted maximum inhibition efficiency was 94.7%, which was relatively high inhibiting efficiency according to previous studies [37]. The opti-mized ratio of each component was 19.8% PBTCA, 36.7% ZnSO$_4$, 31.6% PASP, and 11.9% HPAA, which corresponds to 2 mg/L PBTCA, 3.5 mg/L ZnSO$_4$, 3 mg/L PASP, and 1.5 mg/L HPAA. The experimental inhibition efficiency of the optimized inhibitor was 93.3%, in good agreement with the predicted value of 94.7%. The prediction curves of PBTCA, PASP, and HPAA were steeper than that of ZnSO$_4$, indicating that different compounds produced distinctive effects on the inhibition efficiency. The negatively charged functional groups in PBTCA, PASP, and HPAA might react with ferric hydroxyl groups and produce a homogeneous resistive layer on the surface of carbon steel, while Zn^{2+} might play a collaborative role in the formation of the corrosion layer. In the optimized inhibitor, Zn^{2+} was initially adsorbed on the metal surface through strong chemisorption of Zn^{2+}, while other components absorbed via Coulombic attraction to Zn^{2+} sites (cooperative adsorption) [36]. Stabilization of adsorbed zinc ions with other compounds resulted in both high surface coverage and inhibition efficiency.

3.1.2. Scale inhibition performance

Scale inhibition performance was investigated under different concentrations of HPMA and AA-ATMP-HPA (1, 2, and 3 mg/L), in conjuction with the corrosion inhibitor described above. The static inhibi-

Table 2
The obtained corrosion inhibiting efficiency results in mix design experiments

Number	PBTCA (x_1)	ZnSO$_4$ (x_2)	PASP (x_3)	HPAA (x_4)	Inhibiting efficiency (η) (%)
1	0	0	1	0	32.10
2	0	0.3	0.7	0	32.10
3	0	0	0.87	0.13	33.20
4	0	0	0.75	0.25	34.60
5	0	0.26	0.62	0.12	53.40
6	0	0.49	0.38	0.13	54.30
7	0	0.49	0.26	0.25	55.40
8	0	0.25	0.5	0.25	58.20
9	0	0.49	0.51	0	61.40
10	0.12	0	0.74	0.14	65.60
11	0.22	0	0.78	0	66.40
12	0.26	0	0.64	0.1	70.40
13	0.43	0	0.57	0	72.20
14	0.22	0.49	0.29	0	72.20
15	0.43	0.49	0.08	0	74.90
16	0.22	0.25	0.53	0	77.50
17	0.43	0.25	0.32	0	83.40
18	0.12	0.32	0.42	0.14	87.50
19	0.26	0.49	0.15	0.1	88.30
20	0.26	0.2	0.44	0.1	90.50
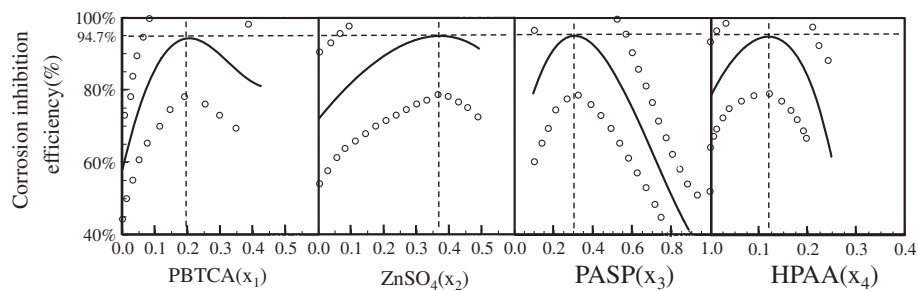
Fig. 2. Profiles of predicted corrosion inhibition efficiencies generated by standard least squares approach which give the optimal corrosion inhibition efficiency obtained from a mixture of four different compounds.

Table 3
The scale inhibiting efficiency under different concentrations of scale inhibitors

Concentrations (mg/L)		Scale inhibiting efficiency (%)		
HPMA	AA-ATMP-HPA	Calcium carbonate (%)	Calcium phosphate (%)	Zinc salt (%)
0	0	55.80	56.70	74.30
1	1	75.30	63.40	80.20
1	2	82.30	74.50	81.30
1	3	87.30	83.40	82.80
2	1	83.50	72.30	81.30
2	2	92.10	77.80	82.20
2	3	95.20	89.30	83.60
3	1	83.40	83.20	82.70
3	2	91.30	90.30	84.10
3	3	94.40	95.30	85.20

tion efficiencies of calcium carbonate, calcium phosphate, and zinc salt scales on carbon steel are shown in Table 3.

The inhibition efficiencies of calcium carbonate and calcium phosphate scales improved by 43.4 and 38.6%, respectively, when concentrations of HPMA or AA-ATMP-HPA were increased from 0 to 3 mg/L, while inhibition of zinc salt scale increased slightly from 74.3 to 85.2%. These results demonstrated that the inhibitor inhibited calcium carbonate and calcium phosphate scales more effectively compared with zinc salt scale.

For calcium carbonate scale, the inhibition efficiencies remained at approximately 80% in all tests, reaching a maximum of 95.2% with 2 mg/L HPMA and 3 mg/L AA-ATMP-HPA. The inhibitor containing 3 mg/L HPMA and 3 mg/L AA-ATMP-HPA also achieved good scale inhibition, with an efficiency of 94.4%. The efficiency increased with the addition of AA-ATMP-HPA and HPMA. In case of HPMA, optimal efficiency was achieved at a concentration of 2 mg/L in combination with a certain amount of AA-ATMP-HPA.

Table 4
The cycle of concentration of K in limited carbonate hardness test under different concentrations of scale inhibitors

Concentrations (mg/L)		
HPMA	AA-ATMP-HPA	Cycle of concentration (K)
0	0	1.23
1	1	1.29
2	2	1.38
3	3	1.50
4	4	1.51
5	5	1.51

For calcium phosphate and zinc salt scales, a high amount concentration of inhibitor resulted in a high inhibition efficiency. The maximum inhibition efficiencies of calcium phosphate and zinc salt scales were 95.3 and 85.2%, respectively, at dosages of 3 mg/L HPMA and AA-ATMP-HPA.

Results of the limited carbonate hardness test are shown in Table 4, and demonstrated that the cycle of concentration (K) increased with the addition of AA-
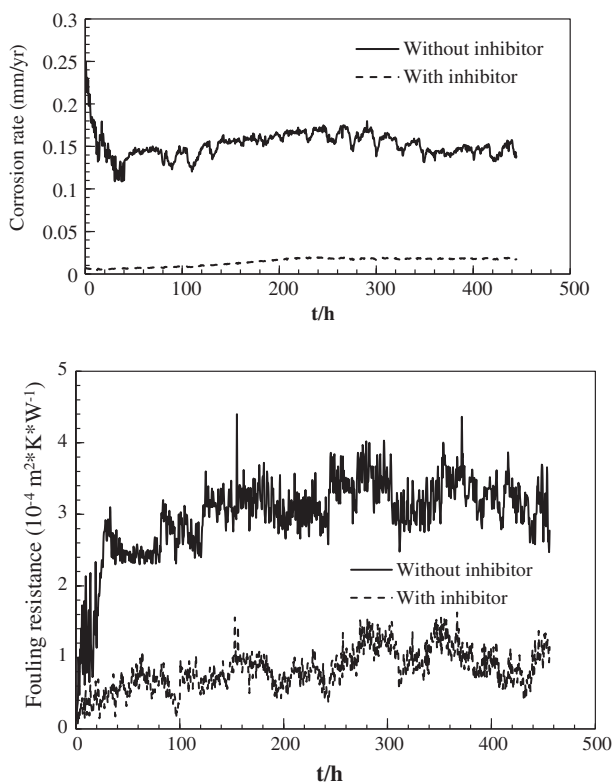
Fig. 3. Dynamics of corrosion rate and fouling resistance in the cooling water in the absence and presence of the inhibitor.

Fig. 4. Changes in water quality parameters in the cooling water in the absence and presence of the inhibitor.

ATMP-HPA and HPMA. A rapid increase occurred in the range of 0–3 mg/L, after which response leveled off up to 5 mg/L. Therefore, 3 mg/L was determined to be the optimal concentration. The highest inhibition was achieved when the inhibitor was comprised of 3 mg/L HPMA and 3 mg/L AA-ATMP-HPA and under these conditions, the inhibition efficiencies of calcium carbonate, calcium phosphate, and zinc salt scales were 94.4, 95.3, and 85.2%, respectively.

3.2. Application of the newly designed inhibitor in a pilot-scale cooling system

Two pilot-scale cooling systems were operated for 20 d using reclaimed wastewater as the cooling water with and without the addition of the designed inhibitor. Corrosion rates of carbon steel and the fouling resistance of system were tested (Fig. 3). Water samples were collected from the makeup water and total alkalinity, Ca^{2+}, and total iron were measured. Dynamic changes in water quality parameters in the cooling water system with and without the inhibitor are shown in Fig. 4.
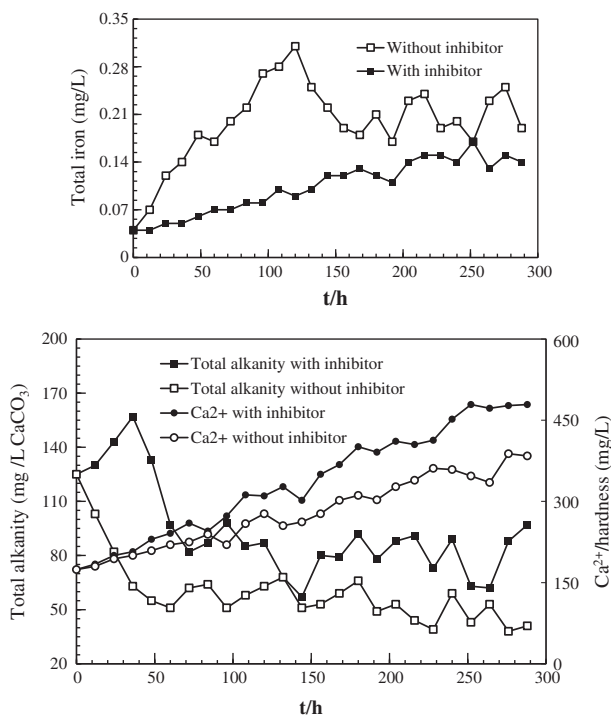
As shown in Fig. 3, the corrosion rate without inhibitor increased to 0.25 mm/yr during the initial 40 h and then decreased to 0.1–0.15 mm/yr under steady-state value. During the initial stage, the corrosion process produced a thick layer of corrosion products. These products were commonly oxides with low diffusion coefficient. Then, the reduction of ions diffusion across the layer could reduce further corrosion and the material reached steady state. With the addition of the inhibitor, the corrosion rate decreased significantly and reached a steady value of 0.015–0.017 mm/yr, indicating good performance of corrosion inhibitor according to the evaluation standard [32]. Fouling resistance was stable at $4 \times 10^{-4} \text{ m}^2 \text{ KW}^{-1}$ after 5 d without addition of the inhibitor, but decreased to $1–1.5 \times 10^{-4} \text{ m}^2 \text{ K W}^{-1}$ with the addition of inhibitor. Low fouling resistance observed following the addition of inhibitor was attributed to the formation of a thin scale layer.

As shown in Fig. 4, total iron concentrations in solutions with and without inhibitor increased initially and then leveled off with slight fluctuation. Total iron concentrations increased during the cycle due to the corrosion process. The average total iron concentration with inhibitor (0.104 mg/L) was considerably lower than that without inhibitor (0.195 mg/L), indicating the corrosion inhibitor effectively reduced iron ion release due
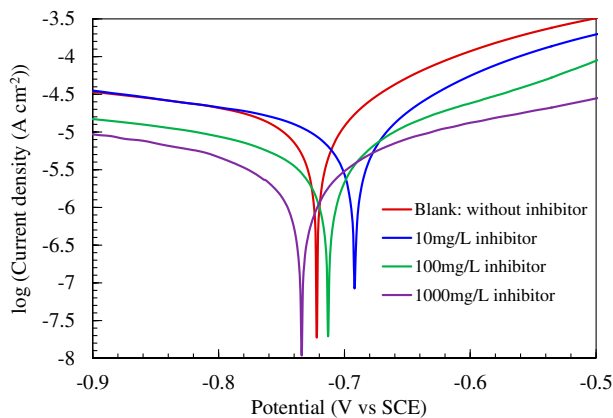
Fig. 5. Potentiodynamic polarization curves of carbon steel in reclaimed wastewater in the absence and presence of the inhibitor with optimized composition of 12.5% PBTCA, 21.8% $ZnSO_4$, 18.7% PASP, 9.4% HPAA, 18.8% AA-ATMP-HPA polymer, and 18.8% HPMA after 30 min immersion at 50°C.

to oxide film development on the carbon steel surface. Value of Ca^{2+} concentration increased more rapidly in the solution with inhibitor than those without inhibitor, due to the ability of inhibitor to prevent the formation of calcium scale by improving calcium dispersability. Total alkalinity decreased initially and then reached a stable level, indicating that the decomposition of bicarbonate (Eq. (11)) in the cooling system was due to the high temperature. In solutions with inhibitor, bicarbonate absorbed inhibitor through a coordination effect [38], resulting in a slight increase in total:

$$2HCO_3^- \rightarrow CO_3^{2-} + CO_2 + H_2O \qquad (11)$$
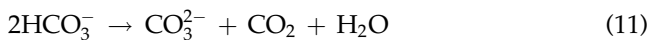
3.3. Electrochemical and SEM studies of corrosion inhibition

Polarization curves of carbon steel in reclaimed wastewater solution at 50°C in the absence and presence of various inhibitor concentrations after 30 min of immersion are shown in Fig. 5. The related electrochemical parameters, corrosion potential (E_{corr}), corrosion current density (i_{corr}), anodic Tafel slope (β_a), and cathodic Tafel slope (β_c), are listed in Table 5.

The cathodic current density of carbon steel decreased significantly with an increase in the inhibitor concentration, indicating that cathodic current density was concentration dependent. These results suggested that in the presence of inhibitor, a protective film adsorbed onto the carbon steel, hindering oxygen diffusion. Similar results were also obtained from anodic reactions, as the anodic current density decreased at a fixed potential. The reduction in anodic process might be due to coverage of the surface with inhibitor. The values of β_c and β_a of carbon steel were found to change with inhibitor concentration, indicate that the inhibitors controlled both the reactions. These results showed that anodic and cathodic processes were hindered in the presence of inhibitor, showing that inhibitor compounds acted as a mixed-type inhibitor.

When compared to the control solution, there was minimal change in the corrosion potential in the presence of 1,000 mg/L inhibitor, whereas a considerable shift in the cathodic direction was observed with 10 and 100 mg/L inhibitor. The corrosion current density was approximately 3–4 times lower in the presence of 100 and 1,000 mg/L inhibitor, compared to the control solution, and one time lower in the presence of 10 mg/L inhibitor. Thus, the inhibition efficiencies increased significantly following an increase in the inhibitor concentrations. The increase in the inhibition efficiency may be attributed to the formation of barrier film which can prevent the reclaimed wastewater from attacking the metal surface. Similar reasons have been given previously to explain the discrepancy in the order of inhibition efficiency by triazole phosphonate derivatives [39].

EIS is a powerful tool which can be used to understand in details the mechanism occurring at the carbon steel/electrolyte interface. Nyquist diagrams of the reclaimed wastewater solution in the presence and

Table 5
Polarization parameters of carbon steel in reclaimed wastewater solution in the absence and presence of the inhibitor with optimized composition of 12.5% PBTCA, 21.8% $ZnSO_4$, 18.7% PASP, 9.4% HPAA, 18.8% AA-ATMP-HPA polymer, and 18.8% HPMA after 30 min immersion

Inhibitor	β_a (mV/dec)	β_c (mV/dec)	i_{corr} (μA/cm^2)	E_{corr} (mV vs. SCE)
Blank	134.4	−376.5	7.923	−722
10 mg/L	127.5	−341.6	5.520	−692
100 mg/L	174.8	−284.9	2.825	−713
1,000 mg/L	191.4	−281.2	1.680	−734
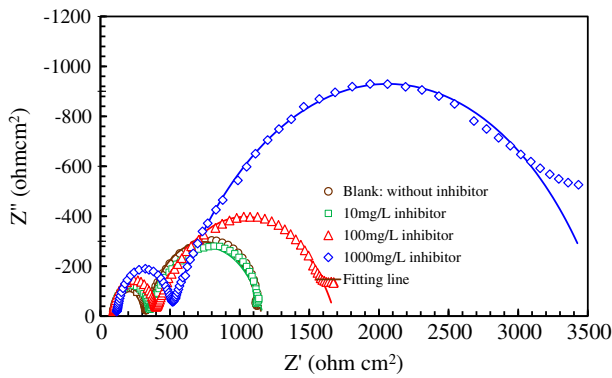
Fig. 6. Nyquist plots for carbon steel in reclaimed wastewater in the absence and presence of the inhibitor with optimized composition of 12.5% PBTCA, 21.8% $ZnSO_4$, 18.7% PASP, 9.4% HPAA, 18.8% AA-ATMP-HPA polymer, and 18.8% HPMA after 30 min immersion at 50°C.
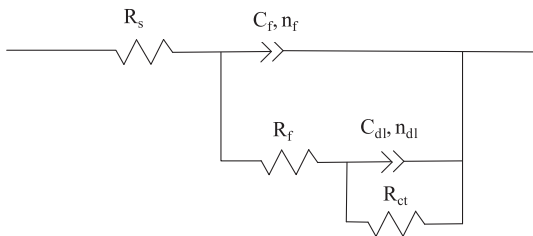
Fig. 7. Equivalent circuit proposed to simulate experimental impedance of carbon steel in the cooling system.

absence of inhibitor are shown in Fig. 6. The impedance measurements were performed under potentiostatic conditions. Before each experiment, the electrode was placed at the open-circuit conditions for 30 min. All impedance spectra exhibited a large capacitive loop in the frequency range of 100–10 mHz. The shape of capacitive loop changed significantly in response to the inhibitor addition. Also shown in Fig. 6, the small semicircle on the high-frequency side ($f > 100$ Hz) which appeared in all solutions, might be related to

the electric double layer. The depressed semicircular appearance in the loop was often attributed to frequency dispersion related to nonhomogeneity or roughness of the solid surface [40].

The EIS curves were fitted according to a typical equivalent circuit shown in Fig. 7, where R_{ct}, the charge transfer resistance, is inversely proportional to the corrosion rate. R_{ct} and C_{dl} are associated with the semicircle in the low-frequency region of Fig. 6, and the resistance R_f and capacitance C_f of the adsorbed inhibitor layer are associated with the semicircle in the high-frequency region. R_f denotes the adsorption film resistance, and C_{dl} and C_f represent the double layer capacitance and adsorption film capacitance, respectively. Instead of capacitance, the constant phase angle element (CPE), is used to account for the heterogeneous electrode surface. The impedance of CPE is expressed as $Z_{CPE} = 1/Y_0(j\omega)^{-n}$, where ω is the angular frequency (in rad s^{-1}) and Y_0 is the CPE constant. The value n is the dispersion coefficient related to the surface inhomogeneity. A decrease in Y_0 suggests an increase in surface roughness [41].

Relevant parameters derived from EIS measurements, as extracted from the equivalent circuit, are shown in Table 6. The values of charge transfer resistance, R_{ct}, increased with the addition of inhibitor, indicating the formation of an insulated adsorption layer. The high values of R_{ct} observed suggested the enhanced inhibitor performance. The double layer capacitance, C_{dl}, was significantly larger in solutions with 10 mg/L inhibitor compared with solutions without inhibitor, in agreement with previous reports [5,15]. The scale and corrosion products tended to increase the real interface area of the electrode, in conjunction with a decrease in C_{dl} in solutions with high concentrations of inhibitor. The decrease in C_{dl} was associated with the gradual replacement of water molecules by the adsorption of inhibitor at the carbon steel/electrolyte interface, resulting in a protective film on the steel surface and preventing mass and charge transfer [42].

Table 6
Electrical elements obtained from the best fitting of experimental impedance diagrams of the carbon steel, using the Zview software

| Inhibitor | R_s (Ω cm^2) | R_f (Ω cm^2) | CPE$_f$ | | R_{ct} (Ω cm^2) | CPE$_{dl}$ | |
			C_f (μF cm^{-2})	n_f		C_{dl} (μF cm^{-2})	n_{dl}
Blank	89.9	237.8	0.276	0.95	832.4	285	0.79
10 mg/L	94.2	258.9	0.283	0.97	815.6	343	0.76
100 mg/L	97.3	301.1	0.185	0.96	1,295.6	265	0.70
1,000 mg/L	118.3	388.7	0.124	0.95	3,115.6	255	0.68
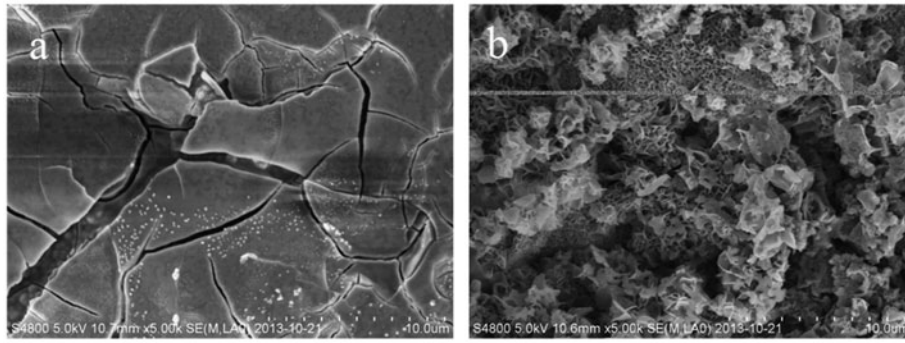
Fig. 8. SEM micrographs of a cast iron surface exposed to reclaimed water (a) with inhibitor and (b) without the inhibitor after a 3 h exposure.
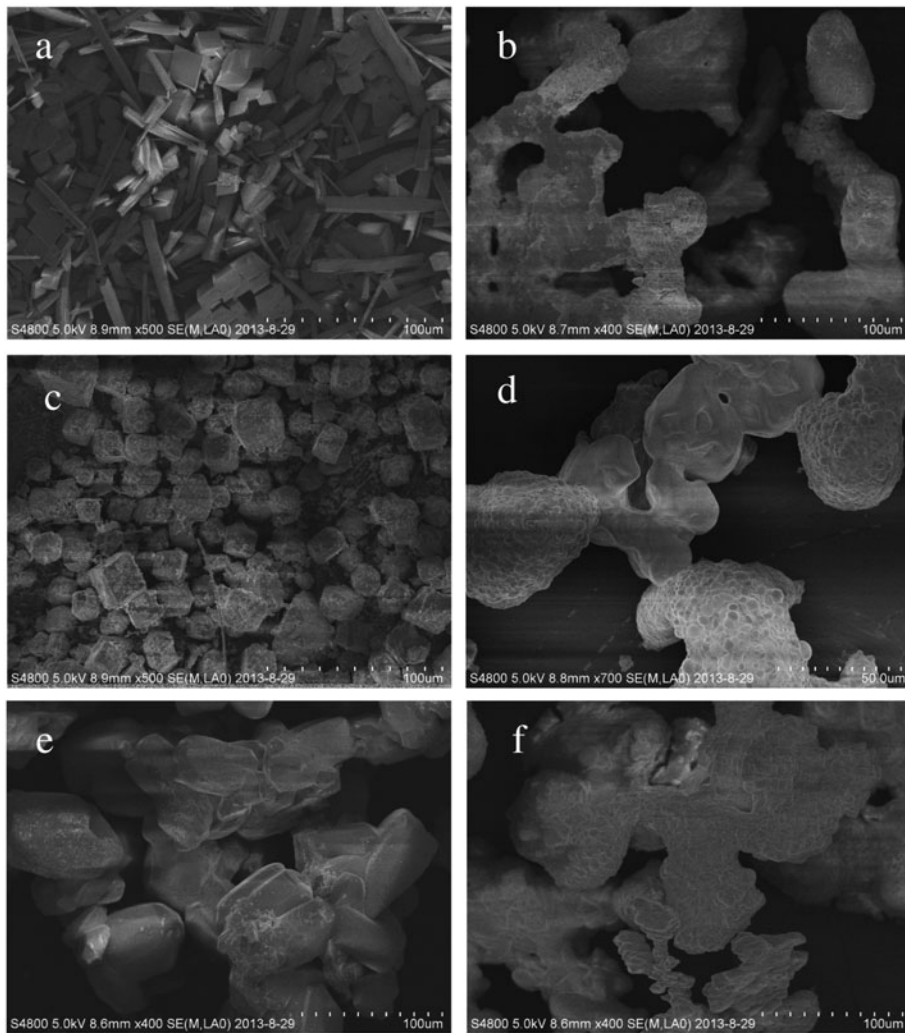
Fig. 9. SEM images of crystals formation: (a) calcium carbonate scale in the absence of inhibitor, (b) calcium carbonate scale in the presence of inhibitor, (c) calcium phosphate scale in the absence of inhibitor, (d) calcium phosphate scale in the presence of inhibitor, (e) zinc salt in the absence of inhibitor, and (f) zinc salt in the presence of inhibitor.
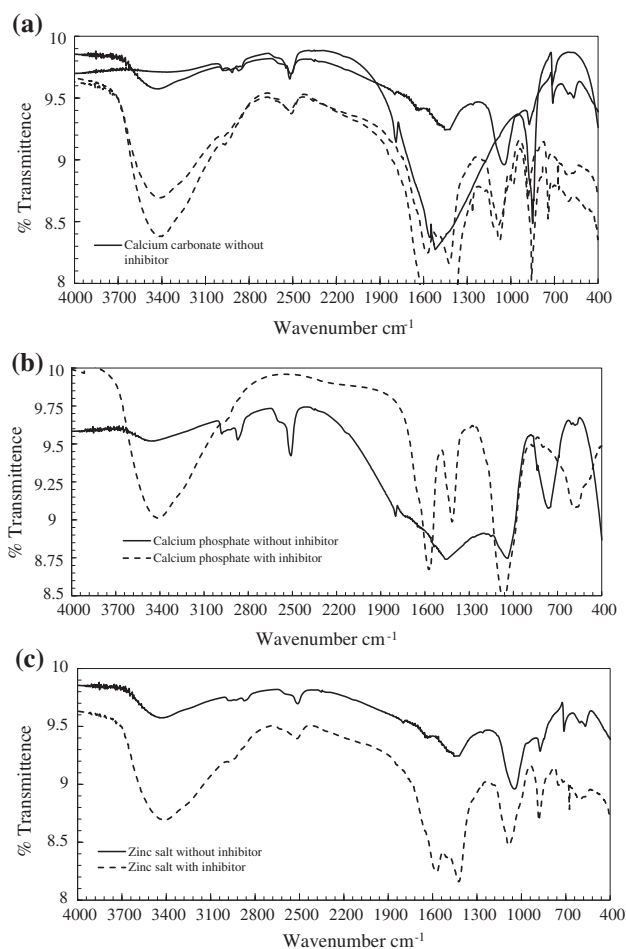
Fig. 10. FTIR spectra of (a) CaCO₃, (b) Ca₃(PO₄)₂, and (c) zinc salt scales in the absence of inhibitor and in the presence of inhibitor.

The phase shift n_{dl} remained nearly constant at a value of approximately 0.7. Value of R_f and C_f described the characteristics of film formation on the metal surface and illustrated the creation of an adsorbed layer in the presence of inhibitor. R_f values increased, while C_f values decreased with the addition of inhibitor, indicating that the ionic conductivity of the surface film decreased with increasing inhibitor concentrations [15].

3.4. SEM and FTIR studies of scale inhibition

A comparison of carbon steel surface with and without the inhibitor after 3 h immersion in the reclaimed wastewater is shown in Fig. 8. Images of surfaces exposed to solutions containing inhibitor (Fig. 8(a)), showed a smooth and dense film on the carbon steel, corroborating with electrochemical results that the formation of an inhibitor film retarded the diffusion of dissolved oxygen. However, the image of surfaces in the absence of inhibitor (Fig. 8(b)) showed a heterogeneous layer comprised of loose scales with a "flower petals" shape, as well as some small globular granules. This could be attributed to thin corrosion layer formation and scales on the carbon steel surface.

SEM images of calcium carbonate, calcium phosphate, and zinc salt scales obtained in the absence and presence of inhibitor at 1,000× magnification are shown in Fig. 9. In Fig. 9(a), blocky, entangled rhombohedral, and needlelike crystals were evident and similar structures were also reported by Wray and Daniel [43]. In the presence of inhibitor (Fig. 9(b)), calcium carbonate scales became more loosely arranged, irregular in shape, and aggravated. Massive cubic calcium phosphate particles were observed in the absence of inhibitor (Fig. 9(c)), while irregualar particles were produced in the presence of inhibitor (Fig. 9(d)). In the zinc salt scale, the morphology of the crystal changed from ball-shaped particles (Fig. 9(e)–(f)) to polymers flocs, indicating that the use of inhibitor had a profound effect on crystal distribution, morphology, and size. All crystals displayed a loss of sharp edges, distorted form, and increase in size. The crystals were unstable, highly dispersive, and easily dissolvable.

It is generally accepted that inhibition of scale formation is influenced by both the location of the adsorbed inhibitor at the crystal surface and the extent of chemical bonding with the surface. High inhibition efficiencies are correlated with high surface binding capacities [44]. The –COO⁻ and –P(O)(OH)₂ groups had a high chelating capacity, and allowed the inhibitor to strongly adsorb onto the crystal [28]. In the newly designed inhibitor, PASP and HPMA contained large numbers of –COO⁻ groups, while PBTCA and AA-ATMP-HPA contained both –COO⁻ and –P(O)(OH)₂ groups These functional groups allowed the inhibitor to adsorb on the crystal surface and bind carboxylic or phosphonate anions to calcium ions, in turn inhibiting the normal growth of inorganic salt crystals. This activity resulted in distortion of crystals and created clusters of large irregular amorphous particles.

The change in crystal forms with the addition of inhibitor was also confirmed by FTIR spectra, as shown in Fig. 10. The characteristic peaks in the scales from carbon steel exposed to inhibitor compared to these without inhibitor were 3,415, 1,564, and 1,415 cm⁻¹. The peak in the frequency of 3,600–3,200 cm⁻¹ was assigned to the hydroxyl group, which contained –P(O)(OH)₂ group [45]. An asymmetrical medium stretching peak at 1,564 cm⁻¹ corresponded to –C=O group of the inhibitor, while absorption at

$1{,}415$ cm^{-1} represented the symmetric stretching of $-COO^-$ group [46]. The spectra of different functional groups were in agreement with results from previous studies [47,48].

It is clear that the inhibitor achieved high efficiency and can be more environment friendly for controlling the corrosion and scale formation. However, the fouling by micro-organisms has attracted great attention for microbiologically influenced corrosion in cooling system [49]. Whether the inhibitor can control the micro-organism of biological fouling in cooling system needs further study.

4. Conclusions

(1) An inhibitor consisting of multiple chemicals displayed a high corrosion inhibition efficiency. Chemicals acted synergistically to prevent corrosion formation on carbon steel surfaces.

(2) The optimized composition of the scale and corrosion inhibitor was 12.5% PBTCA, 21.8% $ZnSO_4$, 18.7% PASP, 9.4% HPAA, 18.8% AA-ATMP-HPA polymer, and 18.8% HPMA, corresponding to 2 mg/L PBTCA, 3.5 mg/L $ZnSO_4$, 3 mg/L PASP, 1.5 mg/L HPAA, 3 mg/L HPMA, and 3 mg/L AA-ATMP-HPA. For this optimized mixture, the inhibition efficiencies of scale and corrosion were 93.3 and 94.4%, respectively.

(3) The inhibitor effectively prevented corrosion and scaling in a pilot-scale system with reclaimed wastewater. The corrosion rate decreased from 0.1 to 0.15 mm/yr to 0.015–0.017 mm/yr and the fouling resistance decreased from 4×10^{-4} m^2 K W^{-1} to 1–1.5×10^{-4} m^2 K W^{-1} with the application of the inhibitor.

(4) A protective film formed by the adsorption of inhibitor onto the surface of the carbon steel prevented corrosion, while interference of crystal formation through the action of carboxyl and phosphonic acid groups prevented scale formation.

Acknowledgments

References

[1] F. Liu, C.C. Zhao, L. Xia, F. Yang, X. Chang, Y.Q. Wang, Biofouling characteristics and identification of preponderant bacteria at different nutrient levels in batch tests of a recirculating cooling water system, Environ. Technol. 32 (2011) 901–910.

[2] G.W. Miller, Integrated concepts in water reuse: Managing global water needs, Desalination 187 (2006) 65–75.

[3] H. Li, M.K. Hsieh, S.H. Chien, J.D. Monnell, D.A. Dzombak, R.D. Vidic, Control of mineral scale deposition in cooling systems using secondary-treated municipal wastewater, Water Res. 45 (2011) 748–760.

[4] E. Ilhan-Sungur, A. Çotuk, Microbial corrosion of galvanized steel in a simulated recirculating cooling tower system, Corros. Sci. 52 (2010) 161–171.

[5] R. Touir, M. Cenoui, M. El Bakri, M.E. Touhami, Sodium gluconate as corrosion and scale inhibitor of ordinary steel in simulated cooling water, Corros. Sci. 50 (2008) 1530–1537.

[6] M.R. Choudhury, M.K. Hsieh, R.D. Vidic, D.A. Dzombak, Corrosion management in power plant cooling systems using tertiary-treated municipal wastewater as makeup water, Corros. Sci. 61 (2012) 231–241.

[7] O. Ghasemi, I. Danaee, G.R. Rashed, M. RashvandAvei, M.H. Maddahy, The inhibition effect of synthesized 4-hydroxybenzaldehyde-1, 3 propandiamine on the corrosion of mild steel in 1 M HCl, J. Mater. Eng. Perform. 22 (2013) 1054–1063.

[8] B. Qian, J. Wang, M. Zheng, B.R. Hou, Synergistic effect of polyaspartic acid and iodide ion on corrosion inhibition of mild steel in H_2SO_4, Corros. Sci. 75 (2013) 184–192.

[9] A. Abulkibash, M. Khaled, B. El Ali, M. Emad, Corrosion inhibition of steel in cooling water system by 2-phosphonobutane-1, 2, 4-tricarboxylic acid and polyvinylpyrrolidone, Arab. J. Sci. Eng. 33 (2008) 29–40.

[10] H. Amar, J. Benzakour, A. Derja, D. Villemin, B. Moreau, T. Braisaz, A. Tounsi, Synergistic corrosion inhibition study of Armco iron in sodium chloride by piperidin-1-yl-phosphonic acid–Zn^{2+} system, Corros. Sci. 50 (2008) 124–130.

[11] M.M. Reddy, A.R. Hoch, Calcite crystal growth rate inhibition by polycarboxylic acids, J. Colloid Interface Sci. 235 (2001) 365–370.

[12] P. Shakkthivel, D. Ramesh, R. Sathiyamoorthi, T. Vasudevan, Water soluble copolymers for calcium carbonate and calcium sulphate scale control in cooling water systems, J. Appl. Polym. Sci. 96 (2005) 1451–1459.

[13] B.D. Mert, M.E. Mert, G. Kardaş, B. Yazıcı, Experimental and theoretical investigation of 3-amino-1, 2, 4-triazole-5-thiol as a corrosion inhibitor for carbon steel in HCl medium, Corros. Sci. 53 (2011) 4265–4272.

[14] C. Zhou, X. Lu, Z. Xin, J. Liu, Corrosion resistance of novel silane-functional polybenzoxazine coating on steel, Corros. Sci. 70 (2013) 145–151.

[15] A. Rochdi, O. Kassou, N. Dkhireche, R. Touir, M. El Bakri, M.E. Touhami, M. Sfaira, B. Mernari, B. Hammouti, Inhibitive properties of 2,5-bis(n-methylphenyl)-1,3,4-oxadiazole and biocide on corrosion, biocorrosion and scaling controls of brass in simulated cooling water, Corros. Sci. 80 (2014) 442–452.

[16] F. Zhang, Y. Tang, Z. Cao, W. Jing, Z. Wu, Y. Chen, Performance and theoretical study on corrosion inhibition of 2-(4-pyridyl)-benzimidazole for mild steel in hydrochloric acid, Corros. Sci. 61 (2012) 1–9.

[17] S.E. Nataraja, T.V. Venkatesha, K. Manjunatha, B. Poojary, M.K. Pavithra, H.C. Tandon, Inhibition of the corrosion of steel in hydrochloric acid solution by some organic molecules containing the methylthiophenyl moiety, Corros. Sci. 53 (2011) 2651–2659.

[18] W. Li, X. Zhao, F. Liu, B. Hou, Investigation on inhibition behavior of S-triazole-triazole derivatives in acidic solution, Corros. Sci. 50 (2008) 3261–3266.

[19] A.L. Kavitha, T. Vasudevan, H.G. Prabu, Evaluation of synthesized antiscalants for cooling water system application, Desalination 268 (2011) 38–45.

[20] J. Roqué, J. Molera, M. Vendrell-Saz, N. Salvadó, Crystal size distributions of induced calcium carbonate crystals in polyaspartic acid and Mytilus edulis acidic organic proteins aqueous solutions, J. Cryst. Growth 262 (2004) 543–553.

[21] G. Zhang, J. Ge, M. Sun, B. Pan, T. Mao, Z. Song, Investigation of scale inhibition mechanisms based on the effect of scale inhibitor on calcium carbonate crystal forms, Sci. China Seri. B: Chem. 50 (2007) 114–120.

[22] W. Sun, L. Wang, T. Wu, G. Liu, α-Mn$_2$O$_3$-catalyzed adsorption reaction of benzotriazole for "smart" corrosion protection of copper, Corros. Sci. 82 (2014) 1–6.

[23] C. Zhou, X. Lu, Z. Xin, J. Liu, Y. Zhang, Polybenzoxazine/SiO$_2$ nanocomposite coatings for corrosion protection of mild steel, Corros. Sci. 80 (2014) 269–275.

[24] J. Telegdi, M.M. Shaglouf, A. Shaban, F.H. Kármán, I. Betróti, M. Mohai, E. Kálmán, Influence of cations on the corrosion inhibition efficiency of aminophosphonic acid, Electrochim. Acta 46 (2001) 3791–3799.

[25] B.A. Rao, M.V. Rao, S.S. Rao, B. Sreedhar, Synergistic effect of N, N-bis (phosphonomethyl) glycine and zinc ions in corrosion control of carbon steel in cooling water systems, Chem. Eng. Commun. 198 (2011) 1505–1529.

[26] Z. Shao, L. Zhang, D. Niu, Y. Zeng, Inhibition and scale prohibiting property of HPMA and ATMP, Corros. Sci. Prot. Technol. 11 (1999) 311–312 (in chinese).

[27] K. Goh, T. Lim, P. Chui, Evaluation of the effect of dosage, pH and contact time on high-dose phosphate inhibition for copper corrosion control using response surface methodology (RSM), Corros. Sci. 50 (2008) 918–927.

[28] B.R. Zhang, L. Zhang, F.T. Li, W. Hu, P.M. Hannam, Testing the formation of Ca–phosphonate precipitates and evaluating the anionic polymers as Ca–phosphonate precipitates and CaCO$_3$ scale inhibitor in simulated cooling water, Corros. Sci. 52 (2010) 3883–3890.

[29] M.K. Hsieh, H. Li, S.H. Chien, J.D. Monnell, I. Chowdhury, D.A. Dzombak, R.D. Vidic, Corrosion control when using secondary treated municipal wastewater as alternative makeup water for cooling tower systems, Water Environ. Res. 82 (2010) 2346–2356.

[30] H. Zhang, C. Dong, L. Bian, Q. Zhao, Experiment study on corrosion control using coking wastewater as circulating cooling water, Earth Sci. Front. 15 (2008) 186–189.

[31] T. Keister, Cooling water management basic principles and technology, ProChemTech International, Inc. Available from: <http://www.prochemtech.com/Literature/Technical/Basic_Cooling_Water_Management_II.pdf>.

[32] Water Treatment Reagent Unit of Standardization Research Institute of Chemical Industry of China, Application Guidebook on Water Quality of Circulation Cooling Water and Standard of Water Treatment Reagents, Chemical Industry Press, Beijing, 2003 (in Chinese).

[33] C.M. Galanakis, G. Fountoulis, V. Gekas, Nanofiltration of brackish groundwater by using a polypiperazine membrane, Desalination 286 (2012) 277–284.

[34] T.E. Larson, R.V. Skold, Laboratory Studies Relating Mineral Quality of Water to Corrosion of Steel and Cast Iron, Illinois State Water Survey, Champaign, 1958.

[35] EPA of China, Test method of Cooling Water Dynamic Simulation, first ed., National Development and Reform Commission, Beijing, 2008 (in chinese).

[36] K. Aramaki, N. Hackerman, Inhibition mechanism of medium-sized polymethylenimine, J. Electrochem. Soc. 116 (1969) 568–574.

[37] M. Finšgar, J. Jackson, Application of corrosion inhibitors for steels in acidic media for the oil and gas industry: A review, Corros. Sci. 86 (2014) 17–41.

[38] Z.H. Shen, J.S. Li, K. Xu, L.L. Ding, H.Q. Ren, The effect of synthesized hydrolyzed polymaleic anhydride (HPMA) on the crystal of calcium carbonate, Desalination 284 (2012) 238–244.

[39] S. Ramesh, S. Rajeswari, Evaluation of inhibitors and biocide on the corrosion control of copper in neutral aqueous environment, Corros. Sci. 47 (2005) 151–169.

[40] P. Bommersbach, C. Alemany-Dumont, J.P. Millet, B. Normand, Formation and behaviour study of an environment-friendly corrosion inhibitor by electrochemical methods, Electrochim. Acta 51 (2005) 1076–1084.

[41] C.H. Hsu, F. Mansfeld, Technical note: Concerning the conversion of the constant phase element parameter Y$_0$ into a capacitance, Corrosion 57 (2001) 747–748.

[42] Z. Tao, W. He, S. Wang, S. Zhang, G. Zhou, A study of differential polarization curves and thermodynamic properties for mild steel in acidic solution with nitrophenyltriazole derivative, Corros. Sci. 60 (2012) 205–213.

[43] J.L. Wray, F. Daniels, Precipitation of calcite and aragonite, J. Am. Chem. Soc. 79 (1957) 2031–2034.

[44] I. Sondi, E. Matijević, Homogeneous precipitation of calcium carbonates by enzyme catalyzed reaction, J. Colloid Interface Sci. 238 (2001) 208–214.

[45] K. Kavita, A. Mishra, B. Jha, Isolation and physicochemical characterisation of extracellular polymeric substances produced by the marine bacterium *Vibrio parahaemolyticus*, Biofouling 27 (2011) 309–317.

[46] F. Freitas, V.D. Alves, J. Pais, N. Costa, C. Oliveira, L. Mafra, L. Hilliou, R. Oliveira, M.A. Reis, Characterization of an extracellular polysaccharide produced by a *Pseudomonas* strain grown on glycerol, Bioresour. Technol. 100 (2009) 859–865.

[47] J.R. Dyer, Application of Absorption Spectroscopy of Organic Compounds, first ed., Prentice Hall, New Delhi, 1965.

[48] R.M. Silverstein, G.C. Bassler, C.T. Morrill, Spectrometric Identification of Organic Compounds, fifth ed., John Wiley & Sons, New York, NY, 1961.

[49] H.B. Wang, C. Hu, X.X. Hu, M. Yang, J.H. Qu, Effects of disinfectant and biofilm on the corrosion of cast iron pipes in a reclaimed water distribution system, Water Res. 46 (2012) 1070–1078.